AGU PUBLICATIONS

Water Resources Research

RESEARCH ARTICLE
10.1002/2013WR015070

Key Points:
- Models of isolated patches are still valid for laterally aligned patches
- The wakes of laterally aligned patches affect their deposition footprint
- A positive feedback for lateral growth of a vegetation patch is identified

Correspondence to:
J. M. Kondziolka,
kondzi@mit.edu

Citation:
Meire, D. W. S. A., J. M. Kondziolka, and H. M. Nepf (2014), Interaction between neighboring vegetation patches: Impact on flow and deposition, *Water Resour. Res.*, *50*, 3809–3825, doi:10.1002/2013WR015070.

Received 21 NOV 2013
Accepted 21 APR 2014
Accepted article online 23 APR 2014
Published online 14 MAY 2014

Interaction between neighboring vegetation patches: Impact on flow and deposition

Dieter W. S. A. Meire[1,2], John M. Kondziolka[2], and Heidi M. Nepf[2]

[1]Department of Civil Engineering, Hydraulics Laboratory, Ghent University, Ghent, Belgium, [2]Department of Civil and Environmental Engineering, Massachusetts Institute of Technology, Cambridge, Massachusetts, USA

Abstract Flow and sedimentation around patches of vegetation are important to landscape evolution, and a better understanding of these processes would facilitate more effective river restoration and wetlands engineering. In wetlands and channels, patches of vegetation are rarely isolated and neighboring patches influence one another during their development. In this experimental study, an adjacent pair of emergent vegetation patches were modeled by circular arrays of cylinders with their centers aligned in a direction that was perpendicular to the flow direction. The flow and deposition patterns behind the pair of patches were measured for two stem densities and for different patch separations (gap widths). The wake pattern immediately behind each individual patch was similar to that observed behind an isolated patch, with a velocity minimum directly behind each patch that produced a well-defined region of enhanced deposition in line with the patch. For all gap widths (Δ), the velocity on the centerline between the patches (U_c) was elevated to a peak velocity U_{max} that persisted over a distance L_j. Although U_{max} was not a function of Δ, L_j decreased with decreasing Δ. Beyond L_j, the wakes merged and U_c decayed to a local minimum. The merging of wakes and associated velocity minimum produced a local maximum in deposition downstream from and on the centerline between the patches. If this secondary region of enhanced deposition promotes new vegetation growth, the increased drag on the centerline could slow velocity between the upstream patch pair, leading to conditions favorable to their merger.

1. Introduction

Macrophytes are important ecosystem engineers [*Jones et al*., 1994] that have a significant effect on both freshwater and marine environments [*Corenblit et al*., 2007; *Dollar*, 2004]. The ecosystem services they provide include decreasing erosion [*Schulz et al*., 2003], reducing turbidity [*Jones et al*., 2012], improving water quality [*Madsen et al*., 2001; *Chambers and Prepas*, 1994], and providing habitat for many species [*Kemp et al*., 2000]. The hydraulic behavior near macrophytes is important, because it influences all of these processes, as well as the evolution of the macrophyte stand.

Traditionally, hydraulic studies have focused on long, uniform meadows, characterizing the bulk flow resistance [e.g., *Kouwen and Unny*, 1975; *Stephan and Gutknecht*, 2002; *Jarvela*, 2005; *Nikora et al*., 2008] and describing the vertical flow structure and turbulence characteristics [e.g., *Lopez and Garcia*, 2001, and review in *Nepf*, 2012]. However, vegetation is often found in patches of finite length and width, rather than continuous segments [*Sand-Jensen and Madsen*, 1992; *Naden et al*., 2006; *Temmerman et al*., 2007; *Schoelynck et al*., 2012], so that recent attention has been focused on the study of finite patches of vegetation, both in the laboratory and in the field [*Cotton et al*., 2006; *Bouma et al*., 2009; *Zong and Nepf*, 2011; *Chen et al*., 2012]. The interaction between neighboring patches has also been considered [*Vandenbruwaene et al*., 2011]. It has been proposed that the feedback between finite patches and flow can lead to large scale, ordered spatial patterns, a process called spatial self-organization [*Rietkerk and Van de Koppel*, 2008]. This mechanism of landscape evolution has been demonstrated for a wide variety of ecosystems, such as mussel beds [*van de Koppel et al*., 2005], diatoms [*Weerman et al*., 2010], vegetation on tidal flats [*van Wesenbeeck et al*., 2008], and vegetation in lowland rivers [*Schoelynck et al*., 2012]. In each case, the introduction of an organism produces positive feedbacks (stress reduction, accumulation of nutrients) and negative feedbacks (stress enhancement, depletion of nutrients), which influence the pattern of growth. For example, *Bouma et al*. [2009] show for intertidal macrophytes (*Spartina anglica*) that, above a certain threshold of vegetation

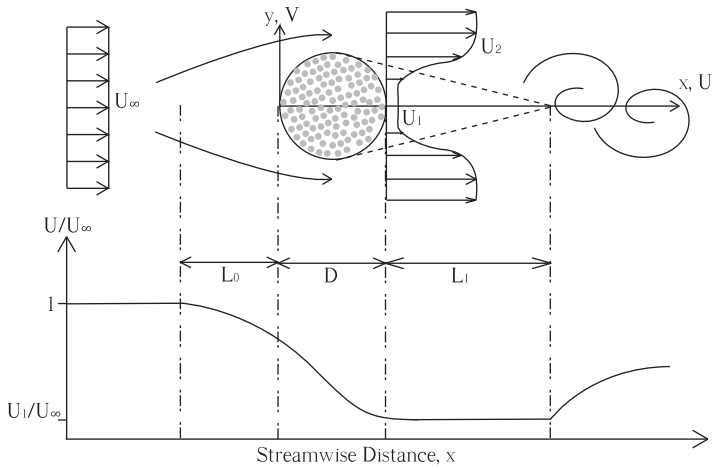

Figure 1. Flow pattern around a porous patch, based on *Zong and Nepf* [2011] and *Chen et al*. [2012]. *D* represents the patch diameter, L_0 represents the length of the upstream adjustment region, L_1 represents the length of the steady wake zone, and *U* and *V* are the streamwise and lateral components of the velocity, respectively. The streamwise coordinate is *x*, and $x = 0$ at the leading edge of the patch. The lateral coordinate is *y*, and $y = 0$ on the patch centerline. U_1 is the streamwise velocity of the slower-moving fluid directly behind the patch ($y = 0$, $x = D$) and U_2 is the streamwise velocity of the faster-moving fluid outside the patch wake ($y > D/2$, $x = D$). The bottom plot depicts the streamwise velocity along the centerline of the patch.

density, sediment is trapped within the vegetation (positive feedback) and erosion is observed next to the vegetation (negative feedback).

In shallow aquatic habitats, where macrophytes can become established, changes in the near-bed velocity will influence sediment transport and thus the bathymetry. These biogeomorphic feedbacks are important to macrophyte development. Sites of erosion are places of lower nutrient availability that lead to less favorable conditions for plant growth [*van Wesenbeeck et al*., 2008]. Sites of deposition, in contrast, are where seeds and organic matter will tend to accumulate, leading to favorable conditions for plant growth [*Gurnell et al*., 2005]. In this study, the bed of the flume is not movable, and as such no bed transport is taken into account. The focus is instead on the deposition of suspended sediments. Deposition of fine sediments in flow influenced by vegetation has been related to the characteristics of the mean and turbulent velocity field through laboratory studies [*Chen et al*., 2012] and field studies [*Sand-Jensen*, 1998; *Cotton et al*., 2006; *Schoelynck et al*., 2012]. *Chen et al*. [2012] modeled patches of emergent vegetation in a laboratory flume. They found that net deposition was generally inhibited in areas of high turbulent kinetic energy (*TKE*) or high velocity, likely due to resuspension, and generally enhanced in areas of low *TKE* and low velocity. In particular, a region of low velocity and low *TKE* occurred directly behind the patch over a length scale of several patch diameters, and enhanced deposition was observed within this region. This is consistent with several field studies. *Schoelynck et al*. [2012] placed model patches of vegetation in a real stream and measured the velocity around the patches. Reduced velocities inside and behind the artificial vegetation allowed for sediment to settle in these areas. *Tanaka and Yagisawa* [2010] and *Tsujimoto* [1999] also observed the deposition of fine material in the wake of individual circular patches. The current work builds on the previous studies of individual patches to consider the interaction between two adjacent patches. We explore how the spacing between vegetation patches influences the pattern of flow distribution and deposition in the wakes of the two patches.

1.1. Previous Work on Flow Adjustment to a Single Patch

To understand how a patch wake is influenced by its neighbor, we must first understand the characteristics of flow past an isolated patch. Flow past an isolated patch is depicted in Figure 1. The patch diameter is *D*, and the patch density is described by *a*, which is the frontal area per unit volume. For a given stem density, *n* (1/cm^2), and mean stem diameter, *d* (cm), $a = n \times d$. U_∞ is the uniform streamwise velocity far upstream of the patch. The streamwise coordinate is *x*, with $x = 0$ at the leading edge of the patch. The lateral coordinate is *y*, with $y = 0$ at the centerline of the patch. The time-averaged velocity in the streamwise and lateral directions is denoted *U* and *V*, respectively. At a distance L_0 upstream of the patch, the flow starts to decelerate and deflect laterally [*Rominger and Nepf*, 2011]. As the fluid passes around and through the patch,

a shear layer forms at each side of the patch between the slower-moving fluid behind the patch (U_1) and the faster-moving fluid outside the patch wake (U_2). The inner edge of each shear layer is depicted with a dashed line in Figure 1. *Zong and Nepf* [2011] showed that the distance from the edge of the patch to the inner edge of the shear layer (δ) grows linearly with streamwise distance (x) from the patch, consistent with free shear layer growth [e.g., *Champagne et al.*, 1976]. The growth rate depends on the velocity difference, $\Delta U = U_2 - U_1$ and the mean velocity within the shear layer, $\bar{U}=0.5\ (U_1 + U_2)$:

$$\frac{d\delta}{dx} = S_\delta \frac{\Delta U}{\bar{U}} \tag{1}$$

S_δ is an empirical parameter equal to 0.10 ± 0.02 for emergent vegetation patches [*Zong and Nepf*, 2011]. The shear layers formed on either side of the patch meet at the patch centerline at a distance L_1 from the patch (Figure 1), where

$$L_1 = \frac{\frac{D}{2}\bar{U}}{S_\delta \Delta U} \tag{2}$$

Over this distance, the velocity on the patch centerline U_1 remains unchanged. This velocity may be predicted from the nondimensional flow blockage, $C_D aD$, where C_D [–] is the drag coefficient for the stems within the patch [*Chen et al.*, 2012]. Beyond this region, ($x > D + L_1$), a von Kármán vortex street may develop, depending on the value of the flow blockage parameter and solid volume fraction (ϕ) [*Zong and Nepf*, 2011]. Specifically, for ϕ less than approximately 4%, vortex streets do not form. When present, the oscillation frequency associated with the patch-scale von Kármán vortex street, f_k, is comparable to that for a solid object of the same diameter, D. Specifically, the Strouhal number $St = f_k D/U_\infty = 0.2$ [*Zong and Nepf*, 2011].

1.2. Review of Flow Adjustment to a Pair of Obstructions

In this study, we consider the flow and deposition patterns near a pair of side-by-side model vegetation patches, each with diameter D. We can draw on some existing literature for side-by-side circular cylinders. The wake characteristics for this geometry depend on the distance between the two cylinders and the Reynolds number ($Re_D = U_\infty D/\nu$), where ν (cm^2/s) is the kinematic viscosity [*Sumner*, 2010]. Three types of flow behavior are summarized by *Sumner* [2010]. When the distance between the two cylinders Δ is larger than 1.2 times the cylinder diameter (D), parallel vortex streets are observed, predominantly in antiphase [*Sumner et al.*, 1999; *Sumner*, 2010]. As the cylinders are brought closer together, and Δ becomes <1.2 times the cylinder diameter, a biased flow pattern develops in which flow through the gap is deflected toward one of the cylinders. The deflection angle of the gap flow increases as Δ/D decreases. The cylinder toward which the flow is deflected has a narrower and shorter near-wake zone and higher frequency shedding than the neighboring cylinder. Finally, at separation distances $<$10–20% of the diameter, the two cylinders behave as a single bluff body, as indicated by the formation of a single von Kármán vortex street that scales with the total width across both cylinders and has a lower frequency of vortex shedding compared with an individual cylinder. The flow between the two cylinders behaves as bleed flow (streamwise flow through the obstruction), which lengthens the streamwise extent of the vortex formation region [*Sumner et al.*, 1999].

The interaction between porous cylinders (a model for vegetation patches) has not been characterized as thoroughly as the interaction of solid cylinders. *Vandenbruwaene et al.* [2011] considered the change in flow distribution close to a pair of vegetation patches. The goal of their study was to understand under what conditions adjacent patches would merge together, rather than remain separated by a channel. Their velocity measurements were taken adjacent to and in between patches of different diameter (D) and different separation distances (Δ). Acceleration of flow, i.e., elevated velocity, between the patches was observed for all conditions; however, the acceleration decreased, compared with the acceleration at the outer edges of the patches, below a gap width $\Delta/D \approx 0.1$. From these observations alone, one might conclude that adjacent patches cannot merge, since flow acceleration, which would tend to promote erosion and inhibit plant growth, will always be maintained in the space between the patches. However, we hypothesize that a different conclusion might be reached if we consider the flow development in the wake of the patches. As

Table 1. Summary of Measurements[a]

D	(cm)	11 ± 0.8	11 ± 0.8	22 ± 0.8	22 ± 0.8
d	(mm)	3.2 ± 0.1	3.2 ± 0.1	3.2 ± 0.1	3.2 ± 0.1
a	(cm^{-1})	0.15 ± 0.02	0.43 ± 0.03	0.13 ± 0.01	0.40 ± 0.01
aD	(–)	1.6	4.8	2.9	8.6
ϕ	(%)	3.7	11	3.3	10
Type		Sparse	Dense	Sparse	Dense
U_∞	(cm/s)	9.5 ± 0.3	9.5 ± 0.3	9.3 ± 0.3	9.2 ± 0.2
Δ	(cm)	0, 1, 2, 3	0, 1, 2, 3	0, 2, 5	0, 2, 5
		4.5, 6, 8	4.5, 6, 8	8, 11, 14	8, 11, 14
		10, 12	10, 12		
Deposition		No	No	Yes	Yes
				$\Delta = 0, 2, 11$ cm	$\Delta = 0, 2, 11$ cm

[a] D is the diameter of the patch, d is the cylinder diameter, a is the frontal area per unit volume, ϕ is the solid volume fraction of the patch, and Δ is the gap distance between the patches.

described above, the wake behind a single patch is a region of sediment deposition and potential vegetation growth. Based on the solid-cylinder literature (above), we anticipate that for some interpatch distances, a merged wake may form behind the pair of patches that resembles the wake of a larger, single patch and, as such, will have a region of enhanced deposition at some point behind and on the centerline between the two patches. Deposition and vegetation growth within the merged wake could eventually influence the flow distribution between the upstream patches and allow the patches to merge. Motivated by this hypothesis, the focus in this study is to determine the influence of interpatch distance, patch density, and patch diameter on the flow and the deposition pattern in the wake of a pair of side-by-side patches.

2. Material and Methods

Measurements were performed in a recirculating flume 16 m long and 1.2 m wide. The flow depth ($H = 14$ cm) was set by a downstream, adjustable weir, and the discharge was set by a variable-speed pump drawing water from the downstream tailbox to the upstream headbox. The discharge was 1000 L/min, resulting in a depth-averaged velocity U_∞ of approximately 10 cm/s.

Circular patches of model vegetation were placed 7 m from the flume entrance. The patches were constructed from wooden dowels and extended through the water surface to mimic emergent vegetation. The dowels had a diameter of $d = 3.2$ mm, a height of 16 cm and were held in a perforated PVC board. The boards consisted of 5.1 holes per square centimeter with centers staggered by 4.8 mm. Tests were performed with patches of two diameters D (11 and 22 cm) at both high and low-flow blockage. The patch density for the high-flow blockage case was $a \approx 0.4$ cm^{-1}, which corresponded to a solid volume fraction of $\phi = (\pi/4)ad \approx 10\%$. For the low-flow blockage case, $\phi \approx 3.3\%$ and $a \approx 0.13$ cm^{-1}. A summary of the different tests is given in Table 1. The distance between the patches Δ (cm) was varied by placing PVC strips of variable width in between the patch boards. The distance Δ was varied from $\Delta/D = 0$ to a maximum of $\Delta/D = 1$.

2.1. Velocity Measurements

Velocity measurements were made using a 3-D Vectrino (Vectrino Velocimeter, Nortek AS), which measures velocity using the acoustic Doppler technique. The sampling volume of the ADV was located at middepth ($z = 7$ cm). Based on vertical profiles of streamwise velocity (data not shown), the velocity did not vary above $z = 6$ cm. The coordinate system is defined with the streamwise coordinate $x = 0$ at the upstream edge of the patches and the lateral coordinate $y = 0$ at the center of the gap between the patches, as shown in Figure 2. Measurements were recorded at a rate of 25 Hz for a period of at least 240 s. The integral time scale (T) was calculated for representative data points and was generally 1–2 s, with a maximum of 11 s within the region of the wake influenced by the von Kármán vortex street, such that the sampling time captured at least $22T$ and generally $180T$, values which the authors found sufficient to determine average characteristics. The data were processed in MATLAB to filter data points that had especially low values in signal to noise ratio (SNR < 15), correlation (corr < 70) or amplitude (amp < 90) [*McLelland and Nicholas*, 2000]. A Doppler noise correction was performed on the data based on the spectral method described in *Voulgaris and Trowbridge* [1998]. The mean time-averaged velocities, respectively (U, V, W) for the (x, y, z) directions, were taken as the average of the remaining measurements over the recording period.

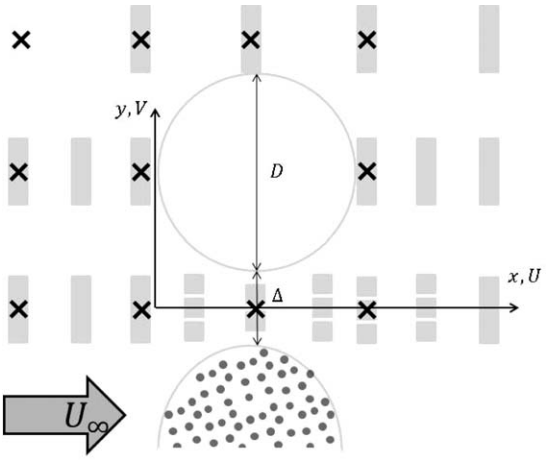

Figure 2. Schematic top-view of flume close to the model vegetation patches (circles), not to scale. The coordinate axis in the horizontal plane is shown, with velocities U and V in the directions of x and y, respectively, with $x = 0$ at the patch leading edge and $y = 0$ on the centerline between the patches. The vertical axis (z) is upward (not depicted). Two patches of diameter D and, separated by a gap Δ, consist of staggered arrays of dowels. The positions of the velocity measurements are indicated by heavy crosses, the positions of the deposition slides are indicated by gray rectangles.

Fluctuations around the mean, denoted u', v', w', were found by subtracting the mean velocity from each instantaneous record. The turbulent kinetic energy per unit mass (*TKE*) was then determined as

$$TKE = \frac{1}{2}\left(\overline{u'^2} + \overline{v'^2} + \overline{w'^2}\right) \quad (3)$$

in which the overbar denotes a time average. Measurements were made from 2.2 m upstream to 5 m downstream of the patches. The measurement positions were spaced more tightly close to the patches.

2.2. Deposition Experiments

Deposition experiments were carried out with a model sediment that was scaled to provide a desired ratio of settling velocity V_s to open-channel bed friction velocity. As this work was motivated by the previously noted feedback between deposition and plant growth [*Gurnell et al.*, 2005], the chosen conditions mimic the transport of organic matter and fine sediment, which produce substrate high in nutrient content and favorable to plant growth. The drag coefficient of the flume bed ($C_f = 0.006$, *White and Nepf* [2007]) was used to estimate an average bed shear velocity of $u^* = 0.7$ cm/s for nonvegetated sections of the flume with uniform flow. Glass sphere particles of 10 micron diameter (Potters Industry, Valley Forge, PA) and a settling velocity $V_s = 0.01$ cm/s were selected, so that $V_s/u^* = 0.014$, which is within the range expected in the field ($V_s/u^* = 0.002$–0.3, see discussion in *Ortiz et al.* [2013]). In addition, the conditions are similar to a previous study [*Zong and Nepf*, 2010], in which clear differences in deposition were observed between the open and vegetated regions of a channel.

Before the start of a deposition experiment, the flume was drained and cleaned to remove sediment that accumulated during previous experiments. Glass microscope slides (VWR VistaVision Microscope Slides) with a small thickness (1 mm) and an area of 7.5 × 2.5 cm or 2.5 × 2.5 cm were thoroughly washed, dried in an oven at 70°C for 4 h, labeled, and then weighed. Slides were placed in 5 longitudinal profiles, partially shown in Figure 2: on the centerline of the gap between the two patches ($y = 0$), on the centerline of each patch ($y = \pm (D + \Delta)/2$), and on the outside edge of each patch ($y = \pm D + \Delta/2$). The longitudinal spacing between the slides was smaller close to the patch and increased with distance from the patch. To begin the experiment, 600 g of sediment (resulting in an initial concentration of ca. 0.13 g/L) was mixed in a small container and the mixture was poured into the tailbox of the flume. The particles were mixed over the flow depth directly when entering the flume and a uniform condition over the flume length was observed within 2 min, based on visual observation. The particles were recirculated in the flume for 4 h. The flow was slowly decelerated to avoid waves, the flume was drained, and then the flume was left to dry for at least 2 days. The slides were baked at 70°C to remove additional moisture and then weighed. The weight difference before and after the experiment is defined as the net deposition (g/cm^2). Three configurations, $\Delta/D = 0.5$, $\Delta/D = 0.1$, and $\Delta/D = 0$, were tested for each patch density. Three repetitions were performed for each set of conditions. A control experiment with no patches in the flume was also performed.

The net deposition mean (μ_{ri}) and standard error (SE_{ri}) of each point were computed using the three replicates for each experimental configuration. To isolate deviations from the mean channel deposition, the mean of each experiment (μ_r) was subtracted from each individual data point. The standard error for the samples in the control experiment (SE_c) was also computed. We considered a point to have enhanced net deposition, relative to the control, if the net deposition differed from the experiment mean by more than the sum of the standard errors:

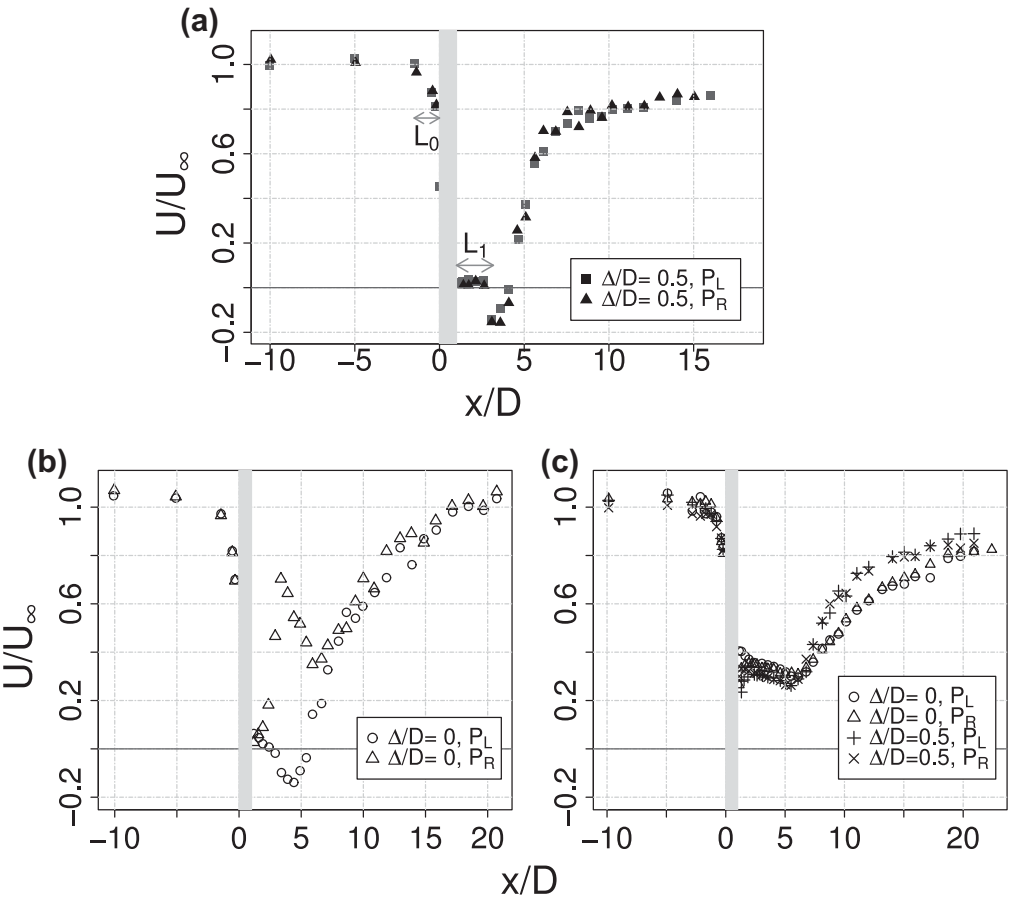

Figure 3. Time-mean, streamwise velocity U normalized by the upstream velocity U_∞, along streamwise coordinate (x) on the patch centerlines. Left-hand and right-hand patches are denoted by P_L and P_R, respectively. The position of the patches is indicated by the gray bar. (a) Dense patches ($D = 22$ cm, $aD = 8.6$, $\phi = 10\%$) with gap width $\Delta/D = 0.5$. L_0 is the upstream adjustment length, and L_1 the steady wake length. The steady wake velocity (U_1) is approximately constant over L_1 followed by a zone of recirculation. (b) Dense patch pair ($D = 22$ cm, $aD = 8.6$, $\phi = 10\%$) with gap width $\Delta/D = 0$. Note asymmetry in wakes. (c) Sparse patch pair ($D = 22$ cm, $aD = 2.9$, $\phi = 3\%$) with gap spacings $\Delta/D = 0$ and 0.5.

$$\mu_{ri} - \mu_r > SE_{ri} + SE_c \tag{4}$$

A spatial, linear interpolation was performed using the algorithm of *Akima* [1978], to obtain contour plots of net deposition.

2.3. Flow Visualization

Characteristics of the wake downstream of the patches were revealed through dye streamlines. Rhodamine WT was injected through a needle oriented parallel to the flow and with an exit velocity that matched the free stream. The positions of the needles were varied to produce streaklines originating from different points upstream and around the patches. Directional lights were clipped to the sides of the flume and directed through the glass sidewalls to avoid water surface reflections and to evenly illuminate the flow depth. The lights extended for a distance of about 1.2 m downstream from the patch. The camera was mounted on a frame upstream of the patches oriented to capture the entire lighted downstream area. Remote capture software was used to avoid disturbing the camera during operation. ImageJ software was used to enhance the contrast and intensity of the dye.

3. Results

3.1. Velocity Profiles on Patch Centerlines

We first consider whether a neighboring patch influences the near field evolution behind each patch by comparing the wakes behind side-by-side patches (Figure 3) with the wake behind an isolated patch. In

Table 2. Steady Wake Velocities U_1 Normalized by the Upstream Velocity U_∞ and Steady Wake Length L_1 for $D = 22$ cm[a]

	Dense		Sparse	
	U_1/U_∞	L_1 (cm)	U_1/U_∞	L_1 (cm)
$\Delta = 0$ cm				
Left	0.03 ± 0.02	75 ± 5	0.34 ± 0.03	101 ± 6
Right	0.04 ± 0.02	12 ± 5	0.33 ± 0.03	100 ± 6
$\Delta = 2$ cm				
Left	0.04 ± 0.02	53 ± 5	0.32 ± 0.03	99 ± 6
Right	0.05 ± 0.03	53 ± 5	0.33 ± 0.02	99 ± 6
$\Delta = 11$ cm				
Left	0.03 ± 0.01	52 ± 5	0.29 ± 0.02	100 ± 6
Right	0.02 ± 0.01	57 ± 5	0.30 ± 0.02	100 ± 6
Single	0.03 ± 0.01*	55 ± 7	0.25 ± 0.05	96 ± 7

[a]The error bars indicate the standard deviation of the velocity measurements within the steady wake zone. The steady wake length L_1 is estimated from longitudinal transects in U, as in *Zong and Nepf* [2011]. The error bars indicate half of the sampling distance between the measurement points. The single patch values are calculated based on equations found in *Chen et al.* [2012] (equations (5) and (6) for the sparse cases). *Indicates that the value is given in *Chen et al.* [2012].

particular, we consider the parameters U_1 and L_1 (described in the Introduction and shown in Figure 1) and evaluate their dependencies on the interpatch distance Δ. The steady wake zone L_1, as defined in *Zong and Nepf* [2011], extends from the trailing edge of the patch to the first measurement point at which the velocity starts to increase. When present, part of the recirculation zone is included, as indicated in Figure 3a. U_1 is the average, streamwise velocity in this zone excluding the recirculation zone, e.g., $U_1/U_\infty = 0.02 \pm 0.01$ for the left patch (P_L) and 0.03 ± 0.01 for the right patch (P_R, Figure 3a). The steady wake length (L_1) and velocity (U_1) were found to be unaffected by the interpatch distance. For the dense patch ($aD = 8.6$), U_1/U_∞ was between 0.02 and 0.05 (Table 2), agreeing within uncertainty with the value of 0.03, found for a single patch of a similar flow blockage [*Chen et al.*, 2012]. Based on observations with isolated patches, *Chen et al.* [2012] proposed a steady wake length for high-flow blockage ($C_D aD > 4$) of $L_1 = 2.5$ (± 0.4) D. In the side-by-side configuration, it is found that $L_1 = 2.4$ (± 0.1) D (Table 2). However, for the case $\Delta = 0$ cm, a strong asymmetry was observed between two high-flow-blockage patch wakes (Figure 3b). Specifically, the gap flow veers toward the right-hand patch (P_R, Figure 3b), shortening L_1 behind the right-hand patch (P_R) and lengthening it behind the left-hand patch (P_L). This deflection of centerline flow is similar to that observed for side-by-side solid cylinders in the Δ/D range of 0.2–1.2, described in the Introduction. This asymmetry is not observed for any other gap spacing. Based on numerical modeling of our experimental setup (J. Janzen, personal communication, 2014), this asymmetry persists even in wider channels, suggesting that it is not related to the presence of the walls.

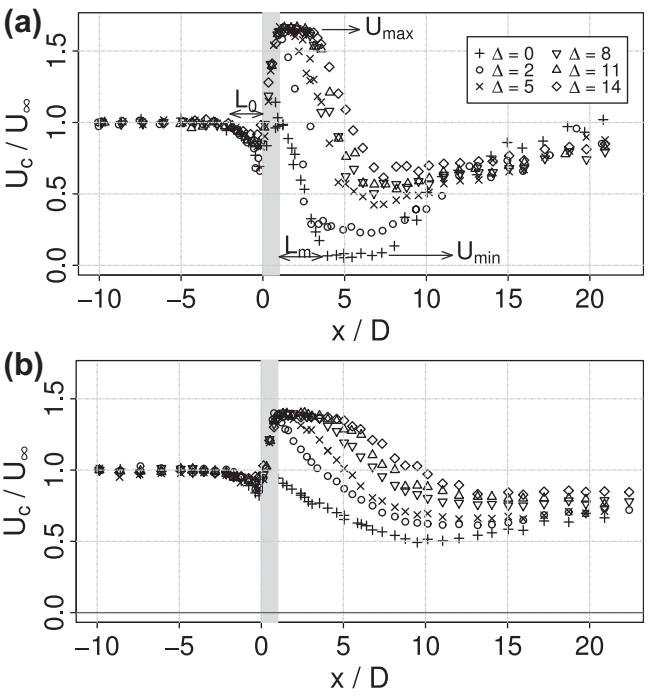

Figure 4. Time-mean, streamwise velocity U normalized by the upstream velocity U_∞, along streamwise coordinate (x) on the centerline between the patches ($y = 0$). The position of the patches is indicated by the gray bar. Gap widths given in the legend are expressed in centimeters. (a) High-flow blockage case ($D = 22$ cm, $aD = 8.6$, $\phi = 10\%$). U_{max} is indicated for all the cases, U_{min} and L_m are indicated for $\Delta = 0$ cm. (b) Low-flow blockage case ($D = 22$ cm, $aD = 2.9$, $\phi = 3.3\%$).

L_1 and U_1 are also independent of the gap width for the sparse

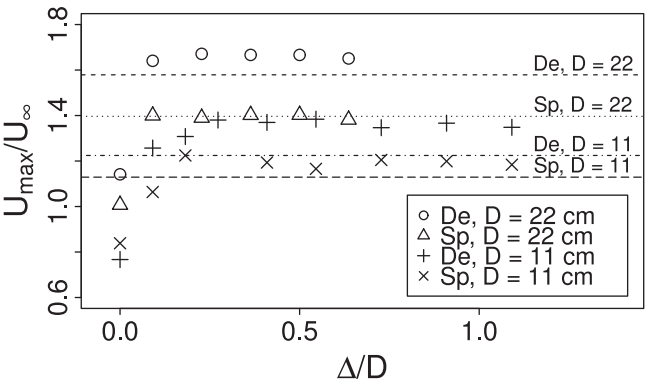

Figure 5. The maximum centerline velocity (U_{max}) is measured at the center of the gap and 5 cm behind the patch pair ($y = 0$, $x = D + 5$ cm). U_{max} is a function of patch diameter ($D = 11$ and 22 cm) and stem density, denoted above as dense (De) and sparse (Sp). U_{max} is only dependent on gap width (Δ) at small values of Δ/D and is essentially constant for $\Delta/D > 0.2$. The uncertainty in the measurements is comparable with the size of the symbols. The lines represent the value of U_{max} calculated with equation (8), using the average U_1/U_∞ given in Table 3 and the geometric features given in Table 1.

patches ($aD = 2.9$, $\phi = 3.3$), as seen in Table 2. Consistent with observations for isolated patches, both L_1 and U_1 are larger for the sparse case than the dense case. In the case of a single patch, *Chen et al*. [2012] proposed the following equations to predict the velocity and length of the near wake region behind low-flow blockage patches, ($C_D aD < 4$):

$$U_1/U_\infty = 1 - 0.26(\pm 0.02) C_D aD \quad (5)$$

$$L_1/D = 2.5\left[\frac{8 - C_D aD}{C_D aD}\right] \quad (6)$$

Assuming $C_D = 1$, equation (5) predicts $U_1/U_\infty = 0.25 \pm 0.05$. This is slightly smaller than the average for all paired cases (0.32 ± 0.02; Table 2), but still in reasonable agreement given the potential error in the assumption $C_D = 1$. Similarly, the length scale L_1 observed behind the paired patches is not affected by gap width and is also in good agreement with the value predicted by equation (6) (96 cm, Table 2). The asymmetry observed in the dense cases at $\Delta = 0$ cm is not observed for any of the sparse cases. This can clearly be seen in Table 2, as L_1 for every patch is equal within uncertainty.

Based on these comparisons (Figure 3 and Table 2), we conclude that the characteristics of the wake directly behind each patch (U_1, L_1) are not affected by a neighboring patch, except in the limit of dense patches approaching zero gap width, and (U_1, L_1) can be predicted from models developed for isolated patches (equations (5) and (6)) [*Chen et al*., 2012].

3.2. Velocity Profiles on Centerline Between Patches

The mean streamwise velocity along the centerline between the patches (U_c) is depicted in Figure 4 for gap widths $\Delta = 0$, 2, 5, 8, 11, and 14 cm ($\Delta/D = 0$–0.6). The profiles are essentially identical upstream of the patches, with deceleration beginning about $L_0 = 2D$ upstream, consistent with L_0 for a single patch of diameter D [*Rominger and Nepf*, 2011; *Zong and Nepf*, 2011]. This suggests that the approaching flow feels the patches as two distinct objects of size D. Note that the upstream adjustment scales on the patch width, with little influence from patch shape, and in particular patch length, as shown specifically in *Rominger and Nepf* [2011]. Similarly, *Vandenbruwaene et al*. [2011] showed that flow adjustment to circular and square patches was not significantly different. In the centerline velocity profiles, the deviation between gap width conditions begins only 1D upstream of the patches. The flow accelerates between the patches, reaching a maximum (U_{max}) directly behind the patches ($x/D = 1$). The maximum centerline velocity is sustained over a distance L_j. The flow on the centerline exiting the gap is similar to a turbulent jet, for which this region of constant, maximal velocity (L_j) is called the potential core [e.g., *Lee and Chu*, 2003]. The potential core is eroded by shear layers growing from either side of the gap toward the gap center. The centerline velocity begins to decelerate when these shear layers meet, which occurs closer to the patch (shorter L_j) as the gap width decreases. In the dense patch cases, the deceleration is followed by a sustained region of minimum velocity (U_{min}) beginning at a distance L_m behind the patch (Figure 4a). Finally, when the shear layers formed at the outermost edges of the patch pair grow to the centerline, the centerline velocity begins to increase. Predictive models for specific regions of the wake evolution are discussed in more detail in the following sections.

3.2.1. Upstream Adjustment Region

The upstream adjustment length, L_0, denotes the distance upstream of the obstruction at which the velocity begins to deviate from its far upstream value. For both porous and solid obstructions L_0 scales with D [*Rominger and Nepf*, 2011; *Belcher et al*., 2003]. We find that, within uncertainty, L_0 is not a function of patch

Table 3. Parameters Describing the Velocity Evolution on the Centerline for Sparse and Dense Patches at Different Gap Distances[a]

Case	L_0 (cm)	U_{max}/U_∞	U_{min}/U_∞	L_j (cm)	L_m (cm)
Dense, $\Delta = 0$	44 ± 5	1.14 ± 0.2	0.07 ± 0.01		87 ± 6
Dense, $\Delta = 2$	41 ± 5	1.64 ± 0.09	0.25 ± 0.02	5 ± 4	75 ± 4
Dense, $\Delta = 5$	42 ± 5	1.67 ± 0.06	0.42 ± 0.03	17 ± 3	111 ± 5
Dense, $\Delta = 8$	37 ± 5	1.66 ± 0.07	0.56 ± 0.03	28 ± 4	134 ± 6
Dense, $\Delta = 11$	36 ± 5	1.66 ± 0.06	0.60 ± 0.04	30 ± 4	135 ± 6
Dense, $\Delta = 14$	37 ± 5	1.65 ± 0.06	0.67 ± 0.03	36 ± 5	149 ± 7
Sparse, $\Delta = 0$	32 ± 5	1.01 ± 0.08	0.49 ± 0.01		209 ± 10
Sparse, $\Delta = 2$	37 ± 5	1.40 ± 0.06	0.61 ± 0.01	6 ± 4	209 ± 10
Sparse, $\Delta = 5$	37 ± 6	1.39 ± 0.06	0.66 ± 0.01	21 ± 3	254 ± 10
Sparse, $\Delta = 8$	32 ± 5	1.40 ± 0.06	0.76 ± 0.01	45 ± 5	290 ± 10
Sparse, $\Delta = 11$	37 ± 5	1.40 ± 0.06	0.80 ± 0.01	67 ± 5	290 ± 15
Sparse, $\Delta = 14$	37 ± 5	1.38 ± 0.06	0.83 ± 0.01	89 ± 5	290 ± 15

[a] L_0 is the upstream adjustment length, U_{max} is the maximum centerline velocity, U_{min} is the minimum centerline velocity, and L_m is the distance from the trailing edge of the patches to the point where the centerline velocity reaches U_{min}. The upstream velocity is $U_\infty = 9.4 \pm 0.3$ cm/s for the dense patches and 9.3 ± 0.3 cm/s for the sparse patches. Gap width in cm.

density or gap width (Figure 4). $L_0 = 40 \pm 4$ cm for dense and 36 ± 3 cm for sparse patches. This corresponds to $L_0 = 1.8$ (± 0.2) D for the dense patches and $L_0 = 1.7$ (± 0.2) D for the sparse patches. These agree within uncertainty with the results of *Rominger and Nepf* [2011] of $L_0 = 2.0$ (± 0.4) D, for a single patch. This suggests that the approaching flow sees each patch as a distinct obstruction, i.e., there is no upstream interaction. It is somewhat surprising that this result holds even for $\Delta = 0$. However, since the patches are circular, even at $\Delta = 0$ preferential flow occurs on the centerline, indicating that hydrodynamically the patches have not effectively merged. The magnitude of the upstream velocity reduction on the centerline has a dependency on the gap width. The velocity reduction is more pronounced for smaller Δ, with a maximum reduction for $\Delta = 0$, and greater for the dense patches (40% reduction from upstream) than for the sparse patches (20%).

3.2.2. Maximum Gap Velocities

The maximum centerline velocity (U_{max}) is shown in Figure 5. At small gap widths the Vectrino probe head could not fit between the two patches. For consistency across all cases, we compare the velocity measured at a specific point: on the gap centerline and 5 cm downstream of the trailing edge of the patch pair ($x = D + 5$ cm). For the larger patches ($D = 22$ cm), U_{max} is the same for all $\Delta/D > 0$, and U_{max} is larger for the denser patches. Again, because of the circular patch shape, flow goes between the patches even for $\Delta/D = 0$, although the magnitude (U_{max}) is diminished relative to $\Delta > 0$ (Figure 5). U_{max} is smaller for the small diameter patches ($D = 11$ cm in Figure 5), because a narrower region of flow is deflected. In addition, $U_{max} < U_\infty$ for $\Delta = 0$. Excluding the $\Delta = 0$ cases, U_{max} is observed to be equal to U_2, the magnitude of velocity on the outermost edge of each patch (see Figures 1 and 9). Similar to the scaling of L_0, discussed above, this further suggests that the flow approaching the patches sees them as individual obstructions, i.e., there is no upstream interaction.

Because this experiment was conducted in a channel, U_{max} can be predicted from mass conservation. Defining the flume width (B),

$$U_\infty HB = U_1 H(2D) + U_{max} H\Delta + U_2 H(B - 2D - \Delta) \tag{7}$$

Using the fact that $U_{max} = U_2$, and solving for U_{max},

$$U_{max} = (U_\infty B - U_1 2D)/(B - 2D) \tag{8}$$

Using measured values of U_∞ and U_1, the values of U_{max} can be predicted from (8), and these predictions are shown as horizontal lines in Figure 5. Excluding the cases of zero gap width, for which $U_{max} \neq U_2$, equation (8) predicts the maximum velocity within 10%, but consistently underestimates, because (8) assumes U_{max} is uniform over Δ, whereas the measured value is taken at the centerline, which is likely a local maximum. Note that (8) may not be valid in a wider channel, since U_2 will eventually decay away from the patches.

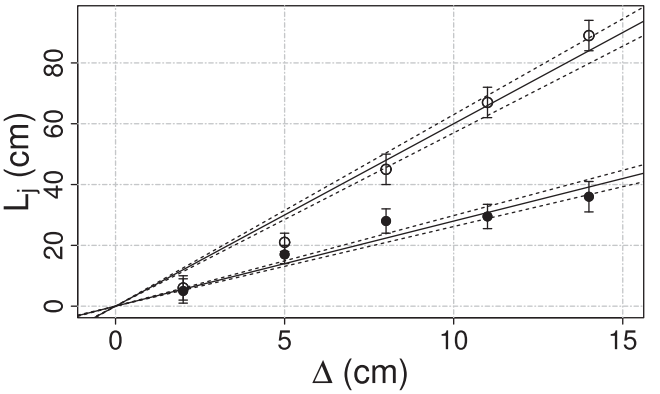

Figure 6. Length of the potential core of the gap jet L_j is a linear function of gap width Δ for the sparse (open circles) and dense patches (solid circles). Physically, we expect L_j to go to zero as the gap width goes to zero, and this constraint is applied to the line fit (equations (9) and (10)) shown with solid lines and the uncertainty with dashed lines.

3.2.3. Potential Core Region

The flow exiting the gap evolves like a jet. In this study, the jet Reynolds number $Re_j = U_j\Delta/\nu$, with $\nu = 10^{-6}$ m^2/s, is always >2000. As such, the jet is turbulent [*Lee and Chu*, 2003]. Close to the nozzle of a jet, there is a wedge-like region of undiminished mean velocity, called the potential core [*Rajaratnam*, 1976]. The length of the potential core, L_j, is linearly dependent on the width of the jet, with typical ratios of 3 to 6 [*Lee and Chu*, 2003; *Rajaratnam*, 1976]. Larger values are noted for jets with a coflow [*Lee and Chu*, 2003]. In this study, the jet width corresponds to the gap width, Δ.

L_j is defined as the distance from the trailing edge of the patches ($x = D$) to the last measurement point where $U_c = U_{max}$ within uncertainty (Table 3). As expected from the analogy with jets, a linear relationship is observed between L_j and Δ (Figure 6). We assume that $L_j = 0$ for $\Delta = 0$. For the dense patches,

$$L_j = 2.8(\pm 0.2)\Delta \qquad (R^2 = 0.91) \tag{9}$$

For the sparse patches,

$$L_j = 6.0(\pm 0.3)\Delta \qquad (R^2 = 0.96) \tag{10}$$

L_j/Δ is greater for the sparse case because U_1, which acts as a co-flow, is higher for the sparse patches.

3.2.4. Deceleration Region

Beyond the distance L_j, the centerline velocity (U_c) decreases (Figure 4), as lower momentum fluid is entrained at the jet edge. For a jet of initial velocity U_{max} and initial width Δ, U_c should evolve as follows [*Giger et al.*, 1991]:

$$\left(\frac{U_{max}}{U_c}\right)^2 = \gamma_u\left(\frac{x}{\Delta} - \frac{x_0}{\Delta}\right) \tag{11}$$

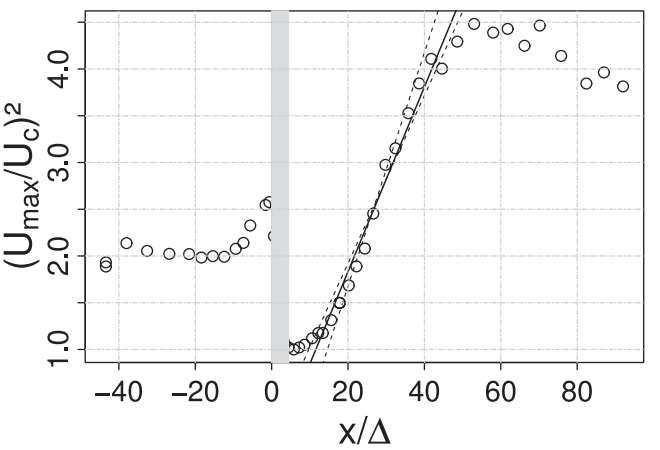

Figure 7. Example of fitting measured centerline velocity, U_c, to the jet spreading model (equation (11)) to obtain the kinematic spreading coefficient γ_u for the sparse patch case with $\Delta = 5$ cm. The result of the best fit for γ_u is 0.099 ± 0.005. The variation in the results, because of point selection, is shown with dashed lines.

γ_u is the kinematic spreading coefficient and x_0 the virtual origin which, for our coordinate system, encompasses the patch diameter (D) and the potential core length (L_j). An example of fitting (11) to the measured values of U_c (Figure 7) clearly shows a region of linear growth for $(U_{max}/U_c)^2$ between $x/\Delta = 5$ and 40, verifying our assumption of jet evolution. The kinematic spreading coefficient γ_u is 0.92 (±0.04) for the dense patches (Table 4). This value is much higher than values in the literature for free planar turbulent jets, which range from 0.13 to 0.21 [*Giger et al.*, 1991; *Rajaratnam*, 1976; *Lee*

Table 4. Kinematic Spreading Coefficients γ_u for the Different Gap Spacings for the Dense ($D = 22$ cm, $\phi = 10$, $aD = 8.6$) and Sparse ($D = 22$ cm, $\phi = 3.3$, $aD = 2.9$) Patches

	Dense Patches	Sparse Patches
Δ (cm)	γ_u	γ_u
2	0.94 ± 0.10	0.042 ± 0.005
5	0.87 ± 0.05	0.099 ± 0.01
8	0.91 ± 0.08	0.121 ± 0.006
11	0.96 ± 0.09	0.140 ± 0.010
14	0.95 ± 0.09	0.138 ± 0.005
Avg.	0.92 ± 0.04	0.11 ± 0.04

and Chu, 2003], meaning that the observed deceleration is faster. This difference is likely due to the difference in turbulence level. *Giger et al*. [1991] report a peak level of turbulence of $u'/U_c \approx 0.25$, whereas for the dense patches the peak value is $u'/U_c \approx 0.5$. The higher level of turbulence contributes to faster mixing which leads to a more rapid deceleration of U_c. Similarly, *Gaskin et al*. [2004] observed that a doubling of the turbulence level increased the spreading coefficient from 0.2 to 2.6. For the sparse patches, $\gamma_u = 0.11$ (± 0.04), which is an order of magnitude less than the dense cases (Table 4), meaning that the observed deceleration is slower. The sparse patch value is in line with values reported by *Giger et al*. [1991] ($\gamma_u = 0.11$) for similar levels of turbulence, $u'/U_c = 0.23$ and 0.25 for present study and *Giger et al*. [1991], respectively.

3.2.5. Centerline Minimum Velocity

At a distance L_m downstream of the patches, the velocity levels off to a constant, minimum value, U_{min} (Figure 4a). The magnitude of U_{min} can be predicted from a simple model that accounts for the mixing of the jet with the lower velocity fluid in the wakes to either side of the jet. The lowest centerline velocity should occur just as the fluid at each wake centerline (the lowest wake velocity) is blended with the jet. This occurs when the blending distance, W_m, extends between the two wake centerlines, $W_m = D/2 + \Delta + D/2 = D + \Delta$. As mixing extends beyond this length scale, higher momentum fluid is added and the centerline velocity will start to increase. From conservation of mass over distance W_m, we can approximate that

$$U_{min}(D+\Delta) = U_1 D + U_{max}\Delta \tag{12}$$

Dividing by U_∞, and noting that for dense patches ($C_D aD > 4$) one can assume $U_1 \ll U_{max}$:

$$\frac{U_{min}}{U_\infty} = \frac{U_{max}(\Delta/D)+U_1}{U_\infty(1+(\Delta/D))} \overset{(C_D aD>4)}{\approx} \frac{U_{max}}{U_\infty}\frac{(\Delta/D)}{(1+(\Delta/D))} \tag{13}$$

As noted above (Figure 5), due to the circular patch geometry, an elevated velocity, U_{max}, occurs at the centerline even when $\Delta = 0$. To account for this, we add an offset (ϵ) to allow for the apparent gap even as Δ goes to zero.

$$\frac{U_{min}}{U_\infty} = \frac{U_{max}((\epsilon+\Delta)/D)+U_1}{U_\infty(1+((\epsilon+\Delta)/D))} \overset{(C_D aD>4)}{\approx} \frac{U_{max}}{U_\infty}\frac{((\epsilon+\Delta)/D)}{(1+((\epsilon+\Delta)/D))} \tag{14}$$

The parameter ϵ is found by fitting (14) to observed values of U_{min} using a nonlinear, least-square estimate employing a Gauss-Newton algorithm; $\epsilon = 1.8$ (± 0.4) cm for the dense patches ($C_D aD = 8.6$) and $\epsilon = 4.8$ (± 0.4) cm for the sparse patches ($C_D aD = 2.9$), shown in Figure 8. Because we expect this offset to be larger for larger mean stem spacing, it makes sense that ϵ is larger for the sparse patches. However, we caution that the parameter ϵ is likely to be case specific, dependent on the shape, density, and homogeneity of the patches. Future work should consider how to predict ϵ from these various factors.

L_m is the distance from the trailing edge of the patches ($x = D$) to the point where the decelerating jet reaches its minimal velocity (U_{min}). For both the sparse and dense patches, L_m increases in a roughly linear fashion with gap width (data in Table 3) and is consistently larger for the sparse cases than the dense cases. Importantly, L_m represents the point at which the two individual patch wakes merge to form a single, larger wake. The two distinct wakes, in the near field, are separated by the gap flow. In the far field, the two wakes merge together to form a single wake. The evolution from a pair of wakes to wake merger is shown through a sequence of lateral transects (Figure 9). For the case shown (dense patches, $\Delta/D = 0.5$), $L_m = 135$ cm. For $x \leq 96$ cm, the elevated centerline velocity separates two distinct and symmetric wakes of lower velocity.

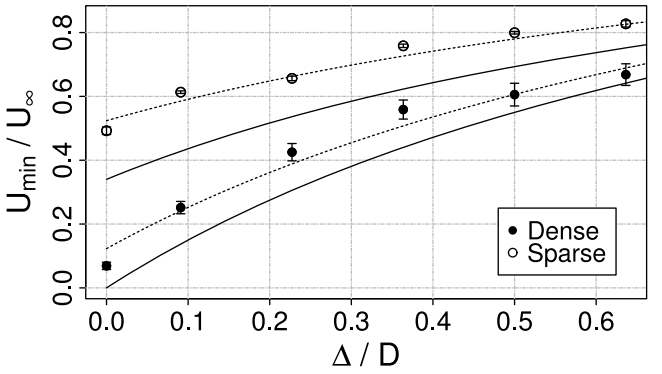

Figure 8. Minimum velocity on the centerline between patches (U_{min}) as a function of gap width (Δ/D, $D = 22$ cm). A simple blending model (equation (13)) provides reasonable agreement (solid line). The agreement is improved by including an offset to the gap width (ϵ in equation (14)). The best fits, shown by dashed lines, yield $\epsilon = 1.8$ cm (dense patches) and $\epsilon = 4.8$ cm (sparse patches).

After L_m, at $x = 160$ cm, the centerline velocity is a minimum, and the velocity profile is consistent with a single wake spanning both patches.

3.2.6. TKE

In section 3.2.4, we noted that the deceleration of the centerline velocity was more rapid between dense patches than between sparse patches due to the higher level of turbulence behind the dense patches. These trends are shown again in Figure 10. For both the dense (open symbols) and sparse (filled symbols) patches, the centerline velocity (circles) decelerates and the patch velocity (triangles) accelerates over the same streamwise distances, $x/D = 3$–5 for dense patches and $x/D = 5$–10 for sparse patches. These regions correspond to peaks in turbulent kinetic energy (*TKE*, Figure 10) associated with the formation of a von Kármán vortex street behind each patch (e.g., Figure 1). The peak *TKE* is significantly higher for the dense patches, consistent with previous studies of isolated patches [*Chen et al*., 2012], and this explains why the deceleration of centerline velocity is more rapid. The dense patches produce a stronger velocity differential ($U_2 - U_1$ in Figure 1), which drives stronger and more coherent von Kármán vortices [*Chen et al*., 2012; *Zong and Nepf*, 2011]. Further, the peak in *TKE* occurs at the same streamwise position both between (center) and in line with (patch) the patches, suggesting that the von Kármán vortices contribute to mixing across the gap. This is also evident in the evolution of dye released from the center of the gap ($y = 0$) and at the outer edge of one patch ($y = \Delta/2 + D$) as shown in Figure 11. Behind the dense patches, both dye traces exhibit lateral oscillations associated with von Kármán vortex streets starting at 80 cm. This corresponds to the peak in *TKE* (Figure 10). Importantly, the lateral traces are synchronized and the lateral excursion is comparable to the total merged wake ($2D + \Delta$). This supports the conclusion that the von Kármán vortex streets contribute to mixing across the gap, enhancing the deceleration of the centerline velocity. The dye traces also indicate that there are two distinct streets (one behind each patch). Although the two vortex streets are synchronized, in phase, the dye traces do not merge into a single vortex. This is consistent with the fact that the observed oscillation frequency (0.1 Hz) scales with the diameter of the single patch, i.e., $f_k \approx 0.2U_\infty/D$ [*Zong and Nepf*, 2011]. Similar trends are observed for the sparse patches, but the von Kármán vortices form further downstream and are less distinct (Figure 11), consistent with their weaker contribution to *TKE* (Figure 10). Finally, in both cases the von Kármán vortex formation occurs at the same position relative to the individual patches as observed behind isolated patches, i.e., at L_1 [*Chen et al*., 2012].

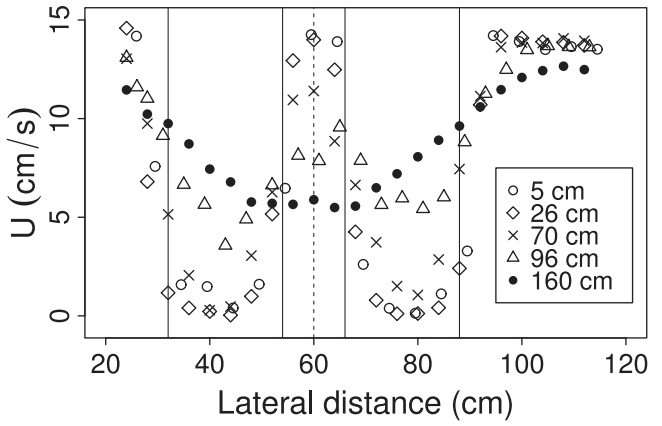

Figure 9. Lateral profiles of streamwise velocity behind two dense patches ($D = 22$ cm) with a gap width of 11 cm. Profiles at distances of 5, 26, 70, 96, and 160 cm (identified in legend) behind the trailing edge of the patch. The dashed, vertical line indicates the centerline between the patches, and the solid vertical lines represent the edges of the patches.

3.3. Deposition

We now connect the main characteristics of the velocity field to the patterns of deposition. In particular, the wake interaction that

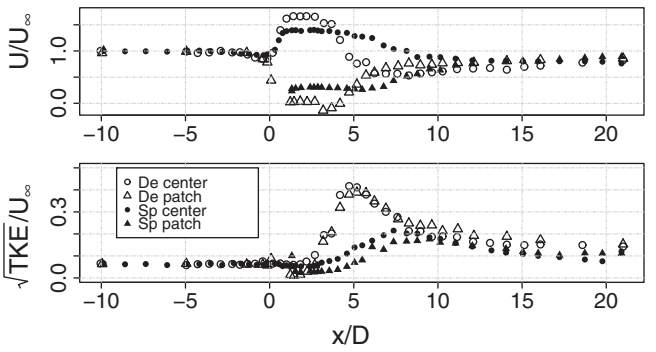

Figure 10. (top) Streamwise velocity (U) and (bottom) turbulent kinetic energy (TKE) versus (middle) streamwise position (x/D) along the centerline between two patches ($y = 0$) and along a patch centerline (patch, $y = (D + \Delta)/2$). Both dense patch (De, $aD = 8.6$) and sparse patch (Sp, $aD = 2.9$) conditions are shown. The gap width is $\Delta/D = 0.5$ and $D = 22$ cm.

produces a local minimum velocity on the centerline between the patches is examined for its potential to enhance deposition. Under control conditions, with no patches in the flume, deposition was uniformly distributed within a variation of 10% and specifically showed no tendency in the streamwise direction, indicating that the deposition was not supply limited (data not shown). With the patches in the flume, distinct patterns of deposition were observed, as shown in Figure 12.

Directly upstream of the patch pair, deposition was enhanced over a distance comparable to the upstream flow adjustment ($L_0 \approx 2\ D$). *Gurnell et al*. [2001] and *Zong and Nepf* [2010] also observed enhanced deposition upstream of a patch, which was attributed to diminished local bed stress due to flow deceleration approaching the patch. Downstream of the patch pairs, three key features can be identified: a zone of enhanced deposition immediately behind each patch, a zone of reduced deposition in between the patches, and a secondary zone of enhanced deposition on the centerline between the patch pair. The zones of enhanced deposition, as defined by equation (4) in the methods, are noted by heavy black lines over the color contours. Behind each patch there is always a zone of higher deposition associated with the individual wake of each patch. The length of this zone (L_{dep}) is reported in Table 5. In most cases, L_{dep} is comparable to the steady wake zone L_1 determined from velocity records (Table 2). For reference, L_1 is also shown in

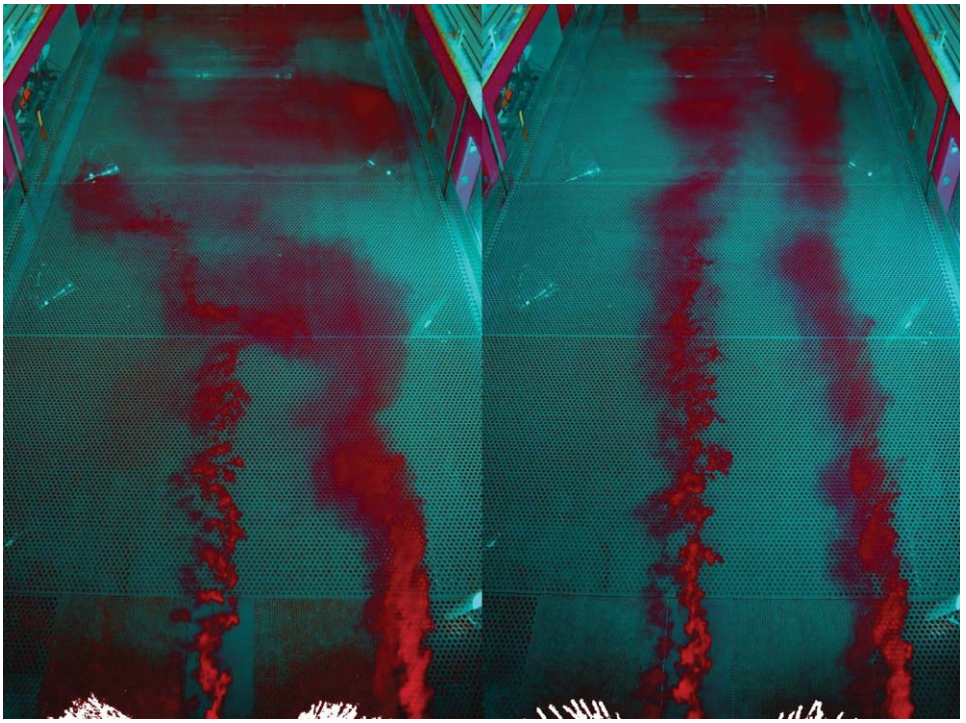

Figure 11. Images of Rhodamine WT injected at the center of the gap between the two patches ($y = 0$) and the edge of one patch ($y = \Delta/2 + D$) at a gap width of $\Delta/D = 0.5$. A dense patch pair (image left) and sparse patch pair (image right) is shown. Flow is from bottom to top. The downstream edge of the patches is just visible in the figure. At 80 cm downstream from the dense patch pair (left image), the tracer reveals the initiation of von Kármán vortex oscillations that span the gap width.

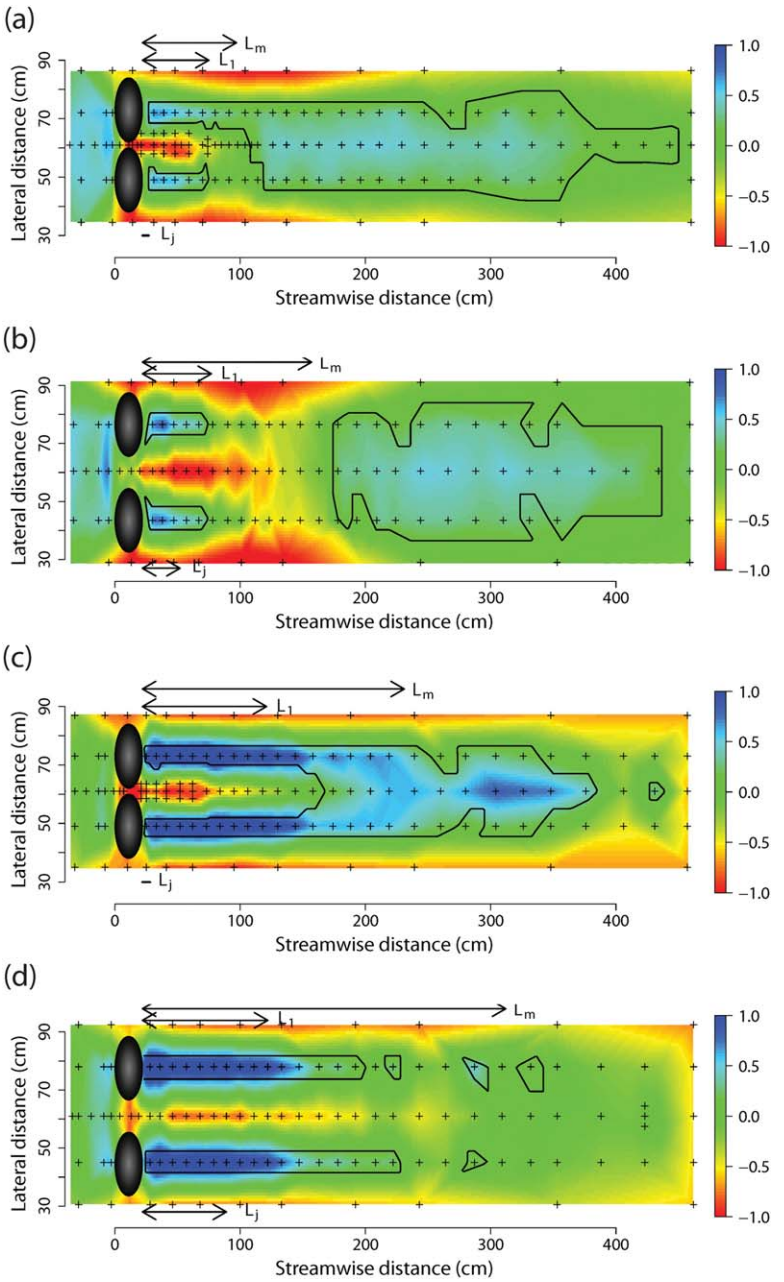

Figure 12. Deposition results for (a) a gap distance of 2 cm ($\Delta/D = 0.1$) for two dense patches, (b) a gap distance of 11 cm ($\Delta/D = 0.5$) for two dense patches, (c) a gap distance of 2 cm ($\Delta/D = 0.1$) for two sparse patches, and (d) a gap distance of 11 cm ($\Delta/D = 0.5$) for two sparse patches. The patches are indicated by the black ovals. Flow direction is from left to right. For each experiment the mean deposition per unit area was subtracted from the measurements such that 0 indicates the average value. Deposition magnitude is in mg/cm^2. The indicated values of L_m, L_j, and L_1 are based on the velocity measurements (summarized in Tables 2 and 3) and measured from the back of the patch. The black contour line indicates the delineation of enhanced deposition based on equation (4).

Figure 12. Only for the sparse case with $\Delta = 11$ cm (Figure 12d) is the deposition clearly longer than L_1. In some cases (marked * in Table 5), the deposition zone L_{dep} merges with the secondary deposition zone (e.g., Figure 12c). Enhanced deposition over the length-scale L_1 has also been observed downstream of individual patches, as described in *Chen et al.* [2012].

Zones of reduced deposition occurred between the patches, as shown in Figure 12 by the red to yellow color between patches. The length of this zone is longer than the potential core in the jet region L_j

Table 5. Overview of the Deposition Measurements[a]

Case	L_{dep} (cm)	$L_{dep,C}$ (cm)
Dense, $\Delta = 0$ cm	44 ± 6*	44 ± 6
Dense, $\Delta = 2$ cm	$47 \pm 6/105 \pm 6$*	105 ± 6
Dense, $\Delta = 11$ cm	47 ± 6	155 ± 7
Sparse, $\Delta = 0$ cm	90 ± 8*	90 ± 8
Sparse, $\Delta = 2$ cm	140 ± 8*	147 ± 8
Sparse, $\Delta = 11$ cm	230 ± 7	

[a] L_{dep} indicates the length of enhanced deposition behind and in line with the individual patches, defined from the trailing edge of the patch. $L_{dep,C}$ indicates the point on the centerline, measured from the trailing edge of the patches, where enhanced deposition is first observed, marking the start of the secondary deposition zone. The uncertainties on L_{dep} and $L_{dep,C}$ are defined by 50% of the distance between the measurement points. The asterisk indicates that the deposition zone in line with the patch connects to the secondary deposition zone. No secondary deposition was observed for Sparse, $\Delta = 11$ cm.

(indicated by arrows in Figure 12). This can be explained by the fact that *TKE* peaks in the deceleration zone and the velocity remains elevated above the control U_∞ for distances longer than L_j. Consistent with this, the region of reduced deposition is longer between the sparse patches compared with the dense patches, because the deceleration of the jet core is slower and extends over a longer streamwise distance.

The zone of secondary deposition on the centerline is a unique feature of the interaction between the two patch wakes. From individual data points, this zone clearly extends laterally between the patch centerlines, and interpolation between points suggests that it extends the width of the two patches and gap ($\Delta + 2D$). The leading edge of this zone moves farther from the patches as the gap increases (e.g., Figures 12a and 12b). $L_{dep,C}$ indicates the distance between the trailing edge of the patches and the start of the secondary deposition zone on the centerline (Table 5). With the dense patches, the secondary deposition zone can easily be recognized and $L_{dep,C}$ is slightly larger than L_m (Table 3), the position of the velocity minimum, which is included in Figure 12 for reference. For the sparse patches it is more difficult to separate the deposition in the individual patch wakes from the deposition in the merged wake, consistent with the less distinct velocity patterns observed for the sparse cases. In contrast to the dense cases, no clear correlation between L_m and a point of increased deposition on the centerline was identified. For the largest gap spacing ($\Delta/D = 0.5$), for which the centerline minimum velocity is the highest, a secondary deposition zone was not observed behind the sparse patches (Figure 12d).

We caution that the results presented here are for a single sediment size, concentration, and flow field. While suggestive of possible deposition patterns, the observed patterns may not be representative of all systems. For example, if the mean velocity is below the threshold for particle motion, a further depression of the velocity in the patch wakes may not lead to enhanced deposition. Similarly, different settling velocities of the sediment (associated with the d_{50} of the sediment) may result in different extents and intensities of the deposition zones.

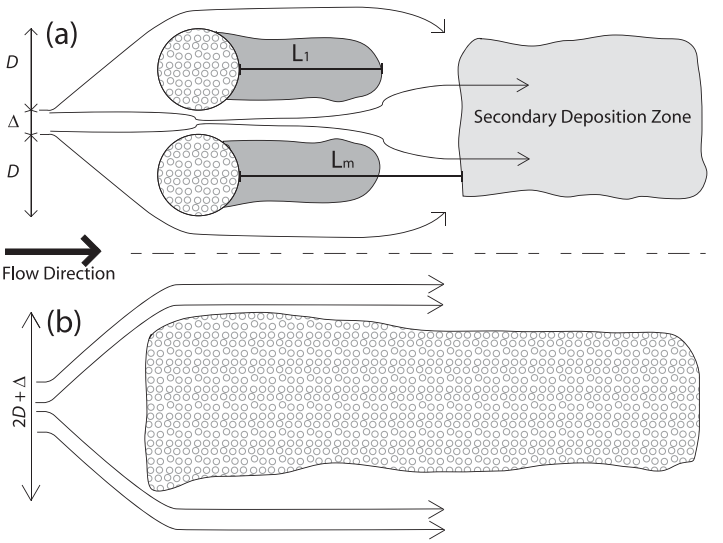

Figure 13. (a) Two patches that are relatively close can create a secondary deposition zone due to the interactions of their wakes that, over time, may cause enhanced growth that leads to (b) patch merger and growth beyond a lateral scale of *D*).

4. Discussion

Our measurements have shown that the velocity and deposition patterns that occur directly behind individual patches are not significantly altered by laterally aligned neighboring patches. Specifically, directly behind each patch there is enhanced deposition that corresponds to a region of diminished mean velocity and turbulence. The length of this region (L_1) increases as the patch density decreases, and it can be predicted from linear shear layer growth [*Zong and Nepf*, 2011]. However, a neighboring patch

can influence the velocity and deposition downstream of L_1. In particular, merging of wakes can produce a velocity minimum on the centerline between the patches at a distance L_m downstream from the patches. The distance L_m is a roughly linear function of gap width (Table 3). The velocity minimum produces a region of enhanced deposition that spans the distance across both patch wakes (Figure 12). The deposition enhancement increases as the minimum velocity decreases, which occurs with increasing patch density and decreasing gap width (Figure 4). This secondary region of deposition may provide a mechanism to foster a merger of the two patches. Consider neighboring patches, with diameters D, as shown in Figure 13a. A first deposition zone occurs immediately behind each patch, corresponding with L_1. Additionally, the interaction of patch wakes leads to a secondary deposition zone on the centerline between the patches. If this secondary zone of enhanced deposition facilitates the establishment and growth of vegetation, it will provide additional drag and flow blockage on the centerline between the original patches, which could reduce or halt the flow between the patches, setting up flow conditions that would allow for patch merger (Figure 13b). Thus, the patches' influence on flow at several diameters downstream produces a positive feedback that may eventually allow the original patches to grow laterally to a merged patch of width $2D + \Delta$ (Figure 13b). Previous descriptions of vegetation-flow feedbacks have identified positive feedbacks only for streamwise patch growth [e.g., *Bouma et al*., 2009] and negative feedbacks for lateral growth. By considering the interaction between neighboring patches we have identified a new, positive feedback for lateral growth.

The strength and location of the secondary deposition zone depends on the flow blockage of the upstream patches and the distance Δ between them. For dense patches, the distance to the start of the secondary zone from the back of the patches, $L_{dep,C}$, is linked to the distance to the minimum centerline velocity (L_m). Using the predictive model for U_c outlined in this study and previous models for isolated patches [*Chen et al*., 2012; *Zong and Nepf*, 2011], the deposition caused by a pair of patches may be predicted, providing a way to incorporate this newly identified feedback into the modeling of landscape evolution.

Acknowledgments
This material is based upon work supported by the National Science Foundation under grants OCE 0751358 and EAR 0738352. Any opinions, findings, and conclusions or recommendations expressed in the material are those of the author(s) and do not necessarily reflect the views of the National Science Foundation. Dieter Meire wants to thank BOF (Bijzonder Onderzoeksfonds, B/10677/02—BOF09/DOC/353) for personal research funding. Data presented in this paper are available upon request from Heidi Nepf at hmnepf@mit.edu.

References

Akima, H. (1978), A method of bivariate interpolation and smooth surface fitting for irregularly distributed data points, *ACM Trans. Math. Software*, *4*(2), 148–164.

Belcher, S., N. Jerram, and J. Hunt (2003), Adjustment of a turbulent boundary layer to a canopy of roughness elements, *J. Fluid Mech.*, *488*, 369–398, doi:10.1017/S0022112003005019.

Bouma, T. J., M. Friedrichs, B. K. van Wesenbeeck, S. Temmerman, G. Graf, and P. M. J. Herman (2009), Density-dependent linkage of scale-dependent feedbacks: A flume study on the intertidal macrophyte Spartina anglica, *Oikos*, *118*(2), 260–268, doi:10.1111/j.1600-0706.2008.16892.x.

Chambers, P., and E. Prepas (1994), Nutrient dynamics in riverbeds: The impact of sewage effluent and aquatic macrophytes, *Water Res.*, *28*(2), 453–464, doi:10.1016/0043-1354(94)90283-6.

Champagne, F., Y. Pao, and I. Wygnanski (1976), 2-Dimensional mixing region, *J. Fluid Mech.*, *74*, 209–250, doi:10.1017/S0022112076001778.

Chen, Z., A. Ortiz, L. Zong, and H. Nepf (2012), The wake structure behind a porous obstruction and its implications for deposition near a finite patch of emergent vegetation, *Water Resour. Res.*, *48*, W09517, doi:10.1029/2012WR012224.

Corenblit, D., E. Tabacchi, J. Steiger, and A. M. Gurnell (2007), Reciprocal interactions and adjustments between fluvial landforms and vegetation dynamics in river corridors: A review of complementary approaches, *Earth Sci. Rev.*, *84*(1–2), 56–86, doi:10.1016/j.earscirev.2007.05.004.

Cotton, J. A., G. Wharton, J. A. B. Bass, C. M. Heppell, and R. S. Wotton (2006), The effects of seasonal changes to in-stream vegetation cover on patterns of flow and accumulation of sediment, *Geomorphology*, *77*(3–4), 320–334, doi:10.1016/j.geomorph.2006.01.010.

Dollar, E. (2004), Fluvial geomorphology, *Prog. Phys. Geogr.*, *28*(3), 405–450, doi:10.1191/0309133304pp419pr.

Gaskin, S., M. McKernan, and F. Xue (2004), The effect of background turbulence on jet entrainment: An experimental study of a plane jet in a shallow coflow, *J. Hydraul. Res.*, *42*(5), 531–540.

Giger, M., T. Dracos, and G. Jirka (1991), Entrainment and mixing in plane turbulent jets in shallow-water, *J. Hydraul. Res.*, *29*(5), 615–642.

Gurnell, A., G. Petts, D. Hannah, B. Smith, P. Edwards, J. Kollmann, J. Ward, and K. Tockner (2001), Riparian vegetation and island formation along the gravel-bed Fiume Tagliamento, Italy, *Earth Surf. Processes Landforms*, *26*(1), 31–62, doi:10.1002/1096-9837(200101)26:1<31::AID-ESP155>3.0.CO;2-Y.

Gurnell, A., K. Tockner, P. Edwards, and G. Petts (2005), Effects of deposited wood on biocomplexity of river corridors, *Front. Ecol. Environ.*, *3*(7), 377–382, doi:10.1890/1540-9295(2005)003[0377:EODWOB]2.0.CO;2.

Jarvela, J. (2005), Effect of submerged flexible vegetation on flow structure and resistance, *J. Hydrol.*, *307*(1–4), 233–241, doi:10.1016/j.jhydrol.2004.10.013.

Jones, C., J. Lawton, and M. Shachak (1994), Organisms as ecosystem engineers, *Oikos*, *69*(3), 373–386, doi:10.2307/3545850.

Jones, J. I., A. L. Collins, P. S. Naden, and D. A. Sear (2012), The relationship between fine sediment and macrophytes in rivers, *River Res. Appl.*, *28*(7), 1006–1018, doi:10.1002/rra.1486.

Kemp, J., D. Harper, and G. Crosa (2000), The habitat-scale ecohydraulics of rivers, *Ecol. Eng.*, *16*(1), 17–29, doi:10.1016/S0925-8574(00)00073-2.

Kouwen, N., and T. Unny (1975), Flexible roughness in open channels, *J. Hydraul. Div. Am. Soc. Civ. Eng.*, *101*(NHY1), 194–196.

Lee, J. H., and V. Chu (2003), *Turbulent Jets and Plumes: A Lagrangian Approach*, Kluwer Academic Publishers, Dordrecht, Netherlands.

Lopez, F., and M. Garcia (2001), Mean flow and turbulence structure of open-channel flow through non-emergent vegetation, *J. Hydraul. Eng.*, *127*(5), 392–402.
Madsen, J., P. Chambers, W. James, E. Koch, and D. Westlake (2001), The interaction between water movement, sediment dynamics and submersed macrophytes, *Hydrobiologia*, *444*(1–3), 71–84, doi:10.1023/A:1017520800568.
McLelland, S., and A. Nicholas (2000), A new method for evaluating errors in high-frequency ADV measurements, *Hydrol. Processes*, *14*(2), 351–366.
Naden, P., P. Rameshwaran, O. Mountford, and C. Robertson (2006), The influence of macrophyte growth, typical of eutrophic conditions, on river flow velocities and turbulence production, *Hydrol. Processes*, *20*(18), 3915–3938, doi:10.1002/hyp.6165.
Nepf, H. M. (2012), Flow and transport in regions with aquatic vegetation, in *Annual Review of Fluid Mechanics*, vol. 44, edited by S. H. Davis and P. Moin, pp. 123–142, Annual Reviews, Palo Alto, Calif., doi:10.1146/annurev-fluid-120710-101048.
Nikora, V., S. Lamed, N. Nikora, K. Debnath, G. Cooper, and M. Reid (2008), Hydraulic resistance due to aquatic vegetation in small streams: Field study, *J. Hydraul. Eng.*, *134*(9), 1326–1332, doi:10.1061/(ASCE)0733-9429(2008)134:9(1326).
Ortiz, A., A. Ashton, and H. Nepf (2013), Mean and turbulent velocity field near rigid and flexible plants, and the implications for deposition, *J. Geophys. Res.*, *118*, 1–15, doi:10.1002/2013JF002858.
Rajaratnam, N. (1976), *Turbulent Jets*, Elsevier Sci., Amsterdam.
Rietkerk, M., and J. Van de Koppel (2008), Regular pattern formation in real ecosystems, *Trends Ecol. Evol.*, *23*(3), 169–175, doi:10.1016/j.tree.2007.10.013.
Rominger, J. T., and H. M. Nepf (2011), Flow adjustment and interior flow associated with a rectangular porous obstruction, *J. Fluid Mech.*, *680*, 636–659, doi:10.1017/jfm.2011.199.
Sand-Jensen, K. (1998), Influence of submerged macrophytes on sediment composition and near-bed flow in lowland streams, *Freshwater Biol.*, *39*(4), 663–679.
Sand-Jensen, K., and T. Madsen (1992), Patch dynamics of the stream macrophyte, Callitriche-Cophocarpa, *Freshwater Biol.*, *27*(2), 277–282, doi:10.1111/j.1365-2427.1992.tb00539.x.
Schoelynck, J., T. De Groote, K. Bal, W. Vandenbruwaene, P. Meire, and S. Temmerman (2012), Self-organised patchiness and scale-dependent bio-geomorphic feedbacks in aquatic river vegetation, *Ecography*, *35*(8), 760–768, doi:10.1111/j.1600-0587.2011.07177.x.
Schulz, M., H. Kozerski, T. Pluntke, and K. Rinke (2003), The influence of macrophytes on sedimentation and nutrient retention in the lower River Spree (Germany), *Water Res.*, *37*(3), 569–578, doi:10.1016/S0043-1354(02)00276-2.
Stephan, U., and D. Gutknecht (2002), Hydraulic resistance of submerged flexible vegetation, *J. Hydrol.*, *269*(1–2), 27–43, doi:10.1016/S0022-1694(02)00192-0.
Sumner, D. (2010), Two circular cylinders in cross-flow: A review, *J. Fluids Struct.*, *26*(6), 849–899, doi:10.1016/j.jfluidstructs.2010.07.001.
Sumner, D., S. Wong, S. Price, and M. Paidoussis (1999), Fluid behaviour of side-by-side circular cylinders in steady cross-flow, *J. Fluids Struct.*, *13*(3), 309–338, doi:10.1006/jfls.1999.0205.
Tanaka, N., and J. Yagisawa (2010), Flow structures and sedimentation characteristics around clump-type vegetation, *J. Hydro-environment Res.*, *4*(1), 15–25, doi:10.1016/j.jher.2009.11.002.
Temmerman, S., T. J. Bouma, J. Van de Koppel, D. Van der Wal, M. B. De Vries, and P. M. J. Herman (2007), Vegetation causes channel erosion in a tidal landscape, *Geology*, *35*(7), 631–634, doi:10.1130/G23502A.1.
Tsujimoto, T. (1999), Fluvial processes in streams with vegetation, *J. Hydraul. Res.*, *37*(6), 789–803.
van de Koppel, J., M. Rietkerk, N. Dankers, and P. Herman (2005), Scale-dependent feedback and regular spatial patterns in young mussel beds, *Am. Nat.*, *165*(3), E66–E77.
van Wesenbeeck, B. K., J. van de Koppel, P. M. J. Herman, and T. J. Bouma (2008), Does scale-dependent feedback explain spatial complexity in salt-marsh ecosystems?, *Oikos*, *117*(1), 152–159, doi:10.1111/j.2007.0030-1299.16245.x.
Vandenbruwaene, W., et al. (2011), Flow interaction with dynamic vegetation patches: Implications for biogeomorphic evolution of a tidal landscape, *J. Geophys. Res.*, *116*, F01008, doi:10.1029/2010JF001788.
Voulgaris, G., and J. Trowbridge (1998), Evaluation of the acoustic Doppler velocimeter (ADV) for turbulence measurements, *J. Atmos. Oceanic Technol.*, *15*, 272–289, doi:10.1175/1520-0426(1998)015<0272:EOTADV>2.0.CO;2.
Weerman, E. J., J. van de Koppel, M. B. Eppinga, F. Montserrat, Q.-X. Liu, and P. M. J. Herman (2010), Spatial self-organization on intertidal mudflats through biophysical stress divergence, *Am. Nat.*, *176*(1), E15–E32, doi:10.1086/652991.
White, B. L., and H. M. Nepf (2007), Shear instability and coherent structures in shallow flow adjacent to a porous layer, *J. Fluid Mech.*, *593*, 1–32, doi:10.1017/S0022112007008415.
Zong, L., and H. Nepf (2010), Flow and deposition in and around a finite patch of vegetation, *Geomorphology*, *116*(3–4), 363–372, doi:10.1016/j.geomorph.2009.11.020.
Zong, L., and H. Nepf (2011), Vortex development behind a finite porous obstruction in a channel, *J. Fluid Mech.*, *691*, 368–391, doi:10.1017/jfm.2011.479.